

# HiRQA: Hierarchical Ranking and Quality Alignment for Opinion-Unaware Image Quality Assessment

Vaishnav Ramesh, Haining Wang, and Md Jahidul Islam

RoboPI laboratory, Department of ECE, University of Florida, US

**Abstract**—Despite significant progress in no-reference image quality assessment (NR-IQA), dataset biases and reliance on subjective labels continue to hinder their generalization performance. We propose HiRQA (Hierarchical Ranking and Quality Alignment), a self-supervised, opinion-unaware framework that offers a hierarchical, quality-aware embedding through a combination of ranking and contrastive learning. Unlike prior approaches that depend on pristine references or auxiliary modalities at inference time, HiRQA predicts quality scores using only the input image. We introduce a novel higher-order ranking loss that supervises quality predictions through relational ordering across distortion pairs, along with an embedding distance loss that enforces consistency between feature distances and perceptual differences. A training-time contrastive alignment loss, guided by structured textual prompts, further enhances the learned representation. Trained only on synthetic distortions, HiRQA generalizes effectively to authentic degradations, as demonstrated through evaluation on various distortions such as lens flare, haze, motion blur, and low-light conditions. For real-time deployment, we introduce HiRQA-S, a lightweight variant with an inference time of only 3.5 ms per image. Extensive experiments across synthetic and authentic benchmarks validate HiRQA’s state-of-the-art (SOTA) performance, strong generalization ability, and scalability. HiRQA model and inference pipeline are available at: <https://github.com/uf-robopi/HiRQA>.

**Index Terms**—Opinion-Unaware Image Quality Assessment, Self-supervised Learning, Ranking.

## I. INTRODUCTION

Image Quality Assessment (IQA) includes computational methods aimed at quantitatively evaluating the perceptual and statistical quality of images, aligning closely with human visual perception. These metrics support a range of computer vision tasks, from content curation to model supervision. While reference-based IQA methods depend on pristine images, such references are rarely available in real-world scenarios, motivating the development of No-Reference IQA (NR-IQA) [52], [54], [55]. NR-IQA plays a critical role in practical applications such as mobile photography, where it guides internal post-processing modules and quality control mechanisms [15], real-time video streaming and enhancement [2], and image restoration pipelines [29], [53] that aim to improve perceptual quality under diverse distortion conditions.

Recent NR-IQA methods have achieved increasingly accurate predictions that align closely with subjective human opinion scores. However, these models often struggle to generalize to unseen distortions or new content, performing poorly on cross dataset evaluation. Furthermore, collecting large-scale opinion-labeled IQA datasets is expensive, and the resulting scores are often subjective and inconsistent, limiting the robustness of supervised methods.

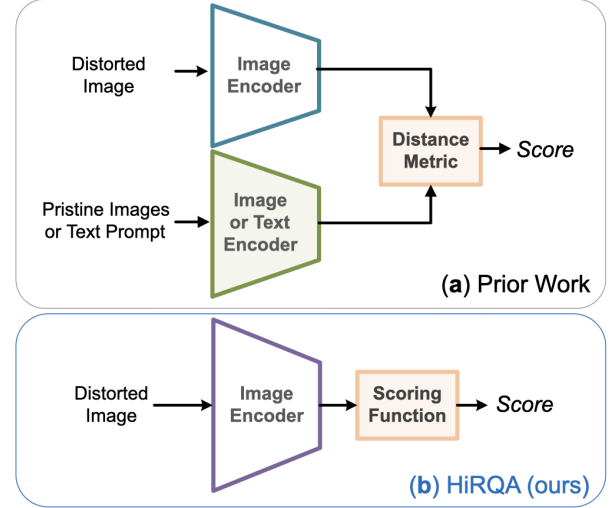


Fig. 1. Existing opinion-unaware IQA methods require additional modalities such as *text prompts* or *pristine* reference images for prediction. In contrast, HiRQA enables SOTA opinion-unaware IQA from the input image alone.

To address these limitations, several Opinion-Unaware IQA (OU-IQA) methods have been proposed. These approaches eliminate the need for human-annotated labels and instead leverage handcrafted statistics [36], [68] or self-supervised signals such as ranking consistency, distortion-specific cues, or large pretrained vision-language models (VLMs). As illustrated in Fig. 1, many existing OU-IQA methods still rely on additional modalities such as a corpus of pristine images or textual prompts during inference. For instance, some methods [5], [36], [68] compute feature distances between a distorted image and a set of pristine natural images, but often fail to generalize to authentically distorted content. On the other hand, VLMs [1], [46], [51] require handcrafted prompts and utilize large text encoders. While text embeddings can be precomputed, the reliance on a large pre-trained text encoder increases the overall model size and introduces modality-specific dependencies, which may limit the scalability and deployment of such methods in real-time or resource-constrained environments. In contrast, we present a simpler approach that answers the following research question:

*How to design an OU-IQA model that can learn to predict perceptual quality using only the input image without any reference images, text prompts, or other modalities at inference time?*

As shown in Fig. 1, our proposed **HiRQA** model learns a hierarchical, quality-aware embedding space using synthetic distortions and relative quality supervision during training. Our

training strategy integrates three complementary losses: (i) a novel pair-of-pairs ranking loss encourages the model to learn a globally consistent quality hierarchy by comparing relative distortion gaps across pairs of images; (ii) an embedding distance loss maps feature distances with perceived quality differences; and (iii) a text-image alignment loss applied only during training, uses structured distortion prompts within a CLIP-based contrastive setup to guide semantic representation.

A comprehensive experimental evaluation of HiRQA on NRIQA benchmark datasets [15], [17], [21], [25], [30], [40], [45], [64] validates the effectiveness of our proposed learning strategy. As shown in Fig 2, HiRQA outperforms most SOTA methods by a large margin, achieving the highest correlation with human visual perception. To also evaluate its generalization to real-world distortions such as lens flare, motion blur, low-light, and atmospheric haze – based on density separation [42]. We assess its performance on unseen enhancement datasets [4], [13], [14], [38], where HiRQA demonstrates a clearer delineation between high- and low-quality samples than state-of-the-art (SOTA) methods.

The main contributions of this paper are as follows:

- 1) We propose HiRQA, a novel opinion-unaware NR-IQA learning pipeline to predict image quality using a single distorted input, without relying on pristine reference images, opinion scores, or text prompts at inference time.
- 2) We introduce a new loss formulation that combines a pair-of-pairs ranking loss and an embedding distance loss. This higher-order supervision strategy enables HiRQA to learn a hierarchical, distortion-aware feature space that aligns well with perceptual quality.
- 3) Extensive experiments on benchmark IQA datasets and detailed ablation studies validate the effectiveness of our proposed training strategy. HiRQA achieves SOTA NR-IQA scores and outperforms existing methods on generalizability for unseen image distortions.

Additionally, we offer a lightweight variant, **HiRQA-S**, which employs a smaller backbone and achieves performance comparable to top-performing models, while having an inference speed of 3.5 milliseconds per image.

## II. BACKGROUND & RELATED WORK

**Traditional Methods.** Non-Reference Image Quality Assessment (NR-IQA) traditionally relied on handcrafted features and statistical models to evaluate image quality without reference images, using subjective IQA databases as proxies for human perception. These methods often leveraged Natural Scene Statistics (NSS) and local descriptors to identify deviations indicative of distortions [16], [18], [35], [37], [43], [60], [62], [63]. While computationally efficient, they exhibited limited robustness when exposed to complex or unseen distortions and often struggled to generalize well. With the emergence of deep learning, Convolutional Neural Networks (CNNs) demonstrated improved performance by learning spatially hierarchical quality-aware features from large-scale data [6], [7], [22], [23], [32], [47], [48], [69], [73]. More recently, transformer-based models have surpassed CNNs by capturing global context and long-range dependencies, which are critical

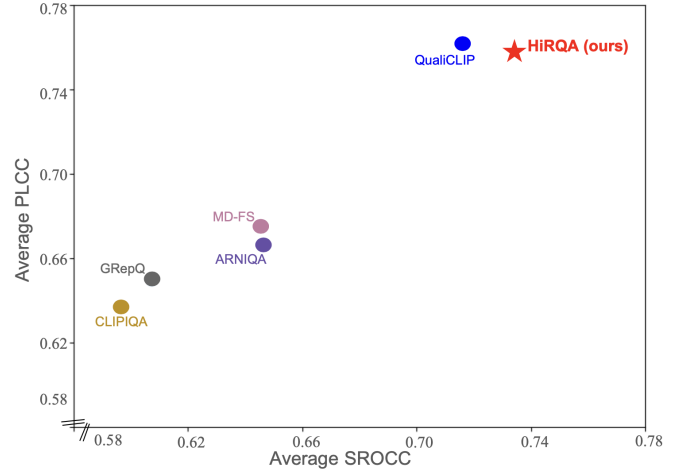


Fig. 2. Average SROCC vs PLCC performance across eight benchmark datasets. HiRQA achieves the highest correlation with human opinion, outperforming other SOTA OU-NRIQA methods.

for perceptual quality understanding [19], [24], [61], [65]. Among these, MANIQA [61] uses multi-dimensional attention mechanisms, achieving SOTA results across the benchmarks.

**Self-supervised Learning.** Self-supervised learning (SSL) has emerged as a compelling alternative for NR-IQA due to its ability to learn quality-aware representations without large-scale annotated datasets [3], [34], [44], [46], [71], [72]. Motivated by the expensive and subjective nature of human opinion scores, SSL aims to leverage intrinsic properties of the data itself such as distortion patterns, ranking consistency, and augmentation invariance to supervise feature learning. Among various SSL strategies, contrastive learning has gained prominence for structuring the feature space to reflect perceptual similarity and distortion sensitivity by bringing similar (positive) pairs closer in the embedding space while pushing apart dissimilar (negative) pairs.

On the other hand, CONTRIQUE [34] uses contrastive learning to align images with similar distortions while separating those with different types, effectively learning distortion-aware feature representations. REIQA [44] adopts MO-COV2 [10] framework with dual encoders to separate content and quality features. ARNIQA [3] employs the SimCLR [9] framework to align distorted views of the same image, allowing the model to learn a distortion-sensitive embedding space while minimizing content bias.

**Vision-Language Modeling.** Textual representations provide rich, high-level semantic context that is inherently interpretable and transferable across tasks. This makes them powerful when paired with visual data. This synergy was first demonstrated by CLIP [41], which aligned images and text in a shared feature space via contrastive learning. By learning to associate visual patterns with natural language, CLIP enabled zero-shot generalization to a wide range of downstream tasks, inspiring a series of vision-language-based approaches for NR-IQA [1], [28], [46], [51], [70], [72].

CLIP-IQA [51] demonstrates that pre-trained vision-language models can assess image quality without supervision by measuring similarity between image embeddings

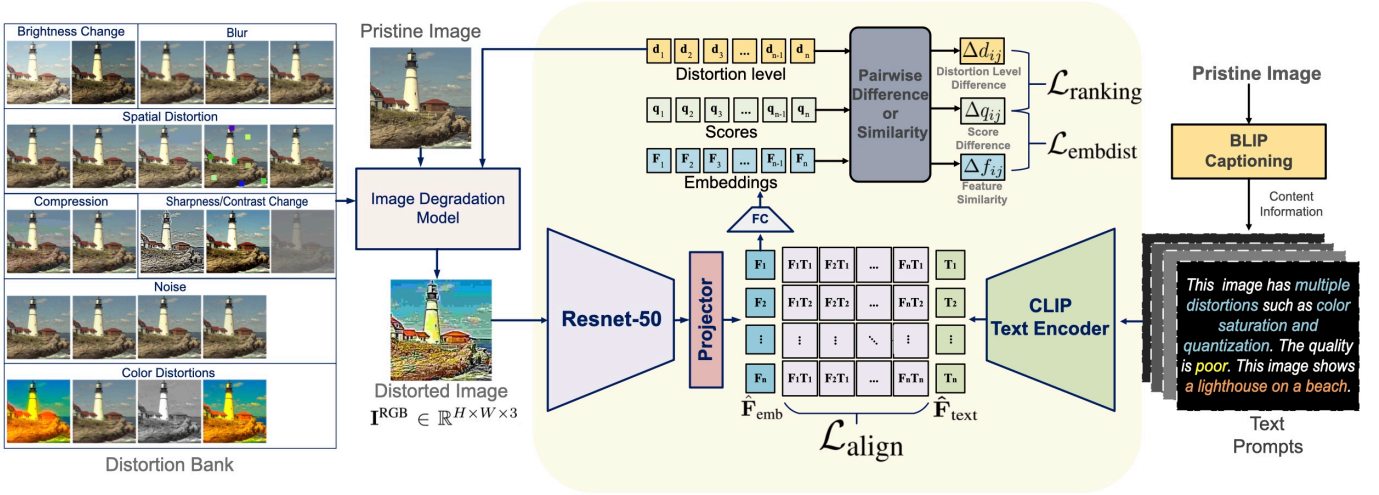


Fig. 3. Training Pipeline of the proposed *HiRQA*, a self-supervised Opinion-Unaware (OU) IQA framework. A ResNet-50 learns distortion-sensitive features from synthetically degraded images. These features are aligned with textual prompts where content information is generated using BLIP-based captioning and encoded via a frozen CLIP text encoder. The model is supervised using three losses: A higher-order pairwise ranking loss, an Image-text alignment loss, and an embedding distance loss capturing perceptual similarity.

and simple prompts such as “a good/bad photo”. Building on this, later methods explored fine-tuning vision-language models to better align with human perceptual judgments. LIQE [70] fine-tunes CLIP in a supervised multi-task setup that jointly predicts image quality, scene type, and distortion type. SLIQUE [72], trained on the TADAC dataset with text annotations describing content, distortions, and appearance, combines self-supervised learning with vision-language alignment through a dual-branch architecture.

Additionally, in Multimodal Large Language Models (MLLMs) for NR-IQA [11], [12], [57]–[59], [66], image inputs are assessed via language-conditioned queries (e.g., “Rate the sharpness of this image”). While these methods enable flexible and instruction-based quality assessment, they require considerable computational resources due to the large model sizes and memory-intensive pipelines.

**Opinion Unaware IQA.** While NR-IQA methods typically rely on subjective opinion scores for supervision, these scores are costly, inconsistent, and prone to dataset bias. OU-IQA aims to bypass this reliance by leveraging statistical regularities or synthetically generated distortions. Early OU-IQA models like NIQE [36] and IL-NIQE [68] employed hand-crafted statistical features, with IL-NIQE enhancing NIQE by incorporating quality-aware features such as Gabor filters and color gradients, comparing distorted image features to a corpus of pristine reference features. MDFS [39] further extended this approach by extracting multiscale features and modeling them using multivariate Gaussian distribution. To better handle authentic distortions, CL-MI [5] proposed a self-supervised contrastive learning framework that explicitly disentangled content and quality information using a mutual information-based loss. However, despite these improvements, their performance remains limited on authentic datasets.

More recent methods leverage vision-language models [1], [46], [51]. GrepQ [46] proposed a dual-encoder design, a fine-tuned CLIP encoder to capture high-level semantics, and a low-level encoder trained with a quality-aware contrastive loss

using perceptual similarity functions as anchors. QualiCLIP [1] built on this by incorporating ranking losses and hand-crafted antonymic prompts to align quality semantics with learned embeddings. While effective, these approaches depend on large pretrained encoders and require additional modalities at inference, limiting scalability.

### III. HiRQA MODEL AND LEARNING PIPELINE

#### A. Model Architecture

The proposed *HiRQA* model aims to learn a distortion-aware and opinion-unaware hierarchical quality representation by leveraging images with known distortion levels. Given an input image  $\mathbf{I}^{RGB} \in \mathbb{R}^{H \times W \times 3}$ , it uses a ResNet-50 [20] backbone to extract deep visual features, which are passed through an attention-based pooling module that projects them into a global embedding vector  $\mathbf{F}_{emb} \in \mathbb{R}^d$ . This vector is then mapped to a quality score  $q \in [0, 1]$  through a fully connected decision layer. The complete end-to-end learning pipeline is illustrated in Fig. 3

*HiRQA*’s primary learning objective is a *higher-order pairwise ranking loss*,  $\mathcal{L}_{ranking}$ , which enforces consistent relative ordering among input images based on their distortion severity. This ranking-based formulation enables the model to learn a perceptual scoring function without requiring subjective human labels. To further structure the learned feature space, we incorporate a contrastive *image-text alignment loss*,  $\mathcal{L}_{align}$  [41] to guide visual features using CLIP-based prompt embeddings (discarded while inference), and an *embedding distance consistency loss*,  $\mathcal{L}_{embdist}$  to encourage that the geometry of the learned embedding space reflects perceptual similarity.

#### B. Loss Functions

1) *Higher-order Pairwise Ranking Loss*: Ranking consistency is a popular self-supervised strategy in OU-IQA. Instead of using subjective opinion scores, the model learns from relative distortion severity among image pairs. *dipIQ* [33]



applies a RankNet-style pairwise ranking loss [8], while QualiCLIP [1] uses a margin loss to rank degraded images of known distortion types.

We build upon the RankNet formulation by introducing the concept of higher-order pairwise ranking. Specifically, we compare the distortion and score differences between the two image pairs. If one pair exhibits a greater distortion gap than another, it should correspondingly show a larger difference in predicted quality scores. This *higher order* comparison ensures a globally consistent and structured ranking across the dataset. The effectiveness of this formulation is validated through ablation studies (Section IV-B), where it outperforms traditional ranking variants.

Let  $q_i$  be the predicted quality scores and  $d_i$  the known distortion levels. From these, we construct all valid image pairs  $(i, j)$  where  $|d_i - d_j| > T_d$ ,  $T_d$  is a threshold to filter out continuous distortion levels which are really similar. Then we compute the absolute distortion and score differences as  $\Delta d_{ij} = |d_i - d_j|$  and  $\Delta q_{ij} = |q_i - q_j|$ . Next, we compare these pairs, denoted  $(i, j)$  and  $(k, l)$ , and define a binary label  $y_{ij,kl}$  to indicate which pair has the greater distortion gap as follows:

$$y_{ij,kl} = \begin{cases} 1 & \text{if } \Delta d_{ij} > \Delta d_{kl} \\ 0 & \text{otherwise.} \end{cases} \quad (1)$$

Each score difference  $\Delta q$  is treated as a logit and supervised using binary cross-entropy (BCE). The higher-order ranking loss,  $\mathcal{L}_{\text{ranknet}}$  is defined over all pair-of-pairs  $\mathcal{S}$  as:

$$\text{BCE}(x, t) = -t \log \sigma(x) - (1 - t) \log(1 - \sigma(x))$$

$$\mathcal{L}_{\text{ranknet}} = \sum_{\mathcal{S}} \frac{\text{BCE}(\Delta q_{ij}, y_{ij,kl}) + \text{BCE}(\Delta q_{kl}, 1 - y_{ij,kl})}{2|\mathcal{S}|}$$

where  $\sigma$  is the sigmoid function. Intuitively, when  $y_{ij,kl} = 1$  (i.e.  $\Delta d_{ij} > \Delta d_{kl}$ ), the model is encouraged to predict a larger score gap  $\Delta q_{ij}$  and a smaller gap  $\Delta q_{kl}$  – effectively aligning score differences with distortion severity. In our implementation, HiRQA performs ranking across batches and gradually learns a consistent ranking structure by comparing image pairs throughout training.

Since we rank absolute score differences, the model may learn either MOS-like (higher score for lower distortion) or DMOS-like behavior. To enforce a consistent MOS interpretation, we introduce a monotonicity regularization term  $\mathcal{L}_{\text{mreg}}$  that penalizes cases where the signed distortion and score differences are aligned, indicating that the model is incorrectly increasing the scores with distortion. Specifically, we minimize the following term:

$$\mathcal{L}_{\text{mreg}} = \frac{1}{N} \sum_{i,j} \log \left( 1 + e^{(q_i - q_j)(d_i - d_j)} \right). \quad (2)$$

The final ranking loss combines the higher-order RankNet loss and the monotonicity constraint:

$$\mathcal{L}_{\text{ranking}} = \mathcal{L}_{\text{ranknet}} + \lambda_{\text{mreg}} \mathcal{L}_{\text{mreg}}. \quad (3)$$

2) *Embedding Distance Consistency Loss*: To reinforce a structured, quality-aware embedding space, we propose an embedding distance consistency loss that formulates contrastive learning as a higher-order ranking problem. Unlike traditional contrastive learning approaches that rely on manually defined hard positive and negative pairs based on class labels or data augmentations, our formulation uses perceptual quality as the basis for supervision. Instead of explicitly specifying which samples are similar or dissimilar, we rank all image pairs according to their predicted quality differences. This allows us to learn a hierarchical representation of image quality, where the embedding space reflects perceptual similarity.

Let  $\hat{\mathbf{F}}_{\text{emb}}$  denote the  $\ell_2$ -normalized image embeddings and  $q_i$  the predicted quality scores. For each pair  $(i, j)$ , the perceptual similarity  $\Delta f_{ij}$  is computed as:

$$\Delta f_{ij} = \exp \left( \frac{\hat{\mathbf{F}}_{\text{emb},i} \cdot \hat{\mathbf{F}}_{\text{emb},j}^\top}{\tau_{\text{emb}}} \right) \quad (4)$$

where  $\tau_{\text{emb}}$  is a learnable temperature parameter. We then align the structure of this space with predicted quality score differences. Following our higher-order ranking framework, we form valid score-distance pairs  $(i, j), (k, l)$  with  $\Delta q_{ij}, \Delta q_{kl} > T_q$ , where  $T_q$  is a threshold that filters out ambiguous or near-identical quality pairs.

This trick prevents noisy supervision and encourages the model to focus on learning from meaningful perceptual differences rather than overfitting to minimal variations that may arise from prediction noise. With a label defined as  $y_{ij,kl} = 1$  if  $\Delta q_{ij} < \Delta q_{kl}$  (Eq. 1), the loss over all pairs of pairs ( $\mathcal{S}$ ) is computed using binary cross-entropy by:

$$\mathcal{L}_{\text{edist}} = \sum_{\mathcal{S}} \frac{\text{BCE}(\Delta f_{ij}, y_{ij,kl}) + \text{BCE}(\Delta f_{kl}, 1 - y_{ij,kl})}{2|\mathcal{S}|}.$$

Moreover, to prevent embedding collapse and promote diversity across feature dimensions, we introduce a covariance regularization term on the normalized embeddings  $\hat{\mathbf{F}}_{\text{emb}}$ . Specifically, we compute the sample covariance matrix  $\Sigma$  and penalize redundancy by minimizing the squared Frobenius norm of its off-diagonal entries. The resulting regularization loss,  $\mathcal{L}_{\text{cov}}$ , is defined as:

$$\mathcal{L}_{\text{cov}} = \frac{1}{D^2} \sum_{i \neq j} \Sigma_{ij}^2, \quad \Sigma = \frac{1}{N-1} (\hat{\mathbf{F}}_{\text{emb}} - \bar{\mathbf{F}})^\top (\hat{\mathbf{F}}_{\text{emb}} - \bar{\mathbf{F}})$$

where  $\bar{\mathbf{F}}$  is the mean and  $D$  is the embedding dimension. Then, the final embedding distance consistency loss is:

$$\mathcal{L}_{\text{embdist}} = \mathcal{L}_{\text{edist}} + \lambda_{\text{cov}} \mathcal{L}_{\text{cov}}. \quad (5)$$

3) *Image-Text Alignment Loss*: To further guide the structure of the quality-aware embedding space, we incorporate an auxiliary image-text alignment loss, inspired by the CLIP framework [41]. We adopt this idea by pairing distorted images with descriptive quality prompts, which provide context about the type of distortion, perceptual quality, and semantic content.

Prior models [51], [70], [72] have demonstrated that using vision-language pretraining can enhance image quality representation. For instance, SLIQUE [72] uses the TADAC dataset,

introduced in the same work, with quality-aware captions during training and discards the text encoder during inference. We follow this design: text prompts are only used at training time to shape the embedding space.

Let  $\hat{\mathbf{F}}_{\text{text}}$  be the normalized embedding of the tokenized prompt from the CLIP text encoder. This loss adopts the standard cross-entropy formulation applied over similarity logits between image and text embeddings. It follows the InfoNCE loss [49] computed as:

$$s_{i,j} = e^{\tau_{\text{align}}} \hat{\mathbf{F}}_{\text{emb},i} \cdot \hat{\mathbf{F}}_{\text{text},j}^{\top}$$

$$\mathcal{L}_{\text{align}} = \frac{-1}{2N} \sum_{i=1}^N \log \frac{\exp(s_{i,i})}{\sum_{j=1}^N \exp(s_{i,j})} + \log \frac{\exp(s_{i,i}^{\top})}{\sum_{j=1}^N \exp(s_{i,j}^{\top})}.$$

The text prompts used here during training are dynamically constructed and follow a consistent structure as follows:

“This photo has {a distortion/multiple distortions} such as {distortion names}. The quality is {quality adjective}. This image shows {semantic caption}.”

Each prompt integrates three components. First, a *distortion clause* describes either a single distortion name or a list of multiple distortions. Second, a *quality-level adjective* is assigned based on the severity of distortion, drawn from the set: {excellent, good, average, poor, bad}. Finally, a *semantic caption* is appended to describe the image content, which is automatically generated using a BLIP-based captioning model [26], [27]. This structured prompting mechanism enables the model to correlate perceptual degradation with both distortion types as well as the underlying semantic context.

### C. Image Degradation Model

Self-supervised NR-IQA methods commonly rely on synthetically degraded images for training. However, training solely on synthetic images limits model generalization to real-world distortions. Prior approaches, such as Re-IQA [44] and CONTRIQUE [34] improve generalization by combining synthetic and authentic images. Moreover, models like QPT [71] and ARNIQA [3] have demonstrated that applying multiple simultaneous distortions to the same image effectively simulates authentic degradations, further boosting generalization.

Our degradation model follows a similar strategy to ARNIQA [3]. Specifically, we utilize 23 distortion types with five intensity levels as defined in the Kadid10k [30] dataset, spanning seven categories: brightness change, blur, spatial distortion, color distortion, compression artifacts, noise, and sharpness/contrast change. For each training sample, we randomly select one or more distortion categories and sequentially apply multiple distortions up to a maximum number  $L_{\text{dist}}$ . In addition to this standard practice, we introduce the concept of “**continuous distortion variation**” by interpolating the intensity between discrete levels, rather than using only fixed levels. This enables us to generate images with subtle quality differences as shown in Fig. 4.

We utilize the 140 K pristine images from the KADIS-700k dataset [31]. We extract random crops from each image and



Fig. 4. Illustration of continuous distortion levels used in our training. The top row shows five discrete levels 1-5 for a particular distortion (Motion Blur), while the bottom row demonstrates continuous levels between levels 4 and 5.

apply degradations to them. For each crop, we first select the distortion types and their base discrete intensity levels  $l$  following ARNIQA [3]. To introduce continuous variation, we sample a small offset  $\delta$  from a zero-mean Gaussian:  $\delta \sim \mathcal{N}(0, \sigma_{\text{off}}^2)$ , which is added to the base level and then clipped to the valid range  $\{1, 5\}$ . The final intensity  $l^* = l + \delta$  is used to linearly interpolate between the nearest discrete levels, generating subtle quality differences within the same nominal distortion category. This augmentation yields a finer spectrum of perceptual qualities, allowing the model to learn from both large and subtle differences.

### D. Training strategy and Inference pipeline

Our training strategy is designed to progressively structure the model’s understanding of image quality, aligning with the hierarchical quality-aware embedding space we aim to learn. In the initial stage, we optimize the model using two objectives: the ranking loss ( $\mathcal{L}_{\text{ranking}}$ ), and the image-text contrastive loss ( $\mathcal{L}_{\text{align}}$ ) to learn a consistent global ranking structure. Then we incorporate the embedding distance loss ( $\mathcal{L}_{\text{embdist}}$ ), which is score-dependent and thus introduced only after the first epoch. This loss refines the learned representation by minimizing feature distances between similarly ranked images and maximizing for dissimilar ones, enabling the model to capture fine-grained perceptual differences. The final training objective is defined as:

$$\mathcal{L}_{\text{final}} = \lambda_{\text{rank}} \mathcal{L}_{\text{ranking}} + \lambda_{\text{align}} \mathcal{L}_{\text{align}} + \lambda_{\text{emb}} \mathcal{L}_{\text{embdist}}$$

where  $\lambda_{\text{emb}} = 0$  during the first epoch and is progressively increased in later epochs.

At inference, HiRQA operates solely on a distorted image, without relying on any auxiliary inputs. As shown in Fig. 5, Quality-aware features extracted by our pretrained backbone

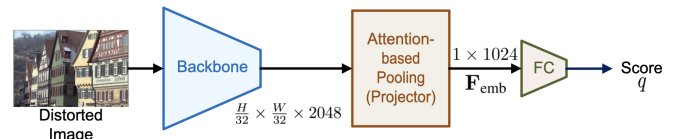


Fig. 5. Inference pipeline of HiRQA. Unlike prior methods, HiRQA requires only a distorted image. Quality-aware features are extracted to predict the quality score  $q$ .

TABLE I

SROCC AND PLCC RESULTS COMPARISON OF HiRQA AGAINST SOTA OPINION-UNWARE (OU) NR-IQA MODELS ON SYNTHETIC AND AUTHENTIC DATASETS ARE SHOWN. THE TOP THREE SCORES ARE MARKED IN BOLDFACED RED, BLUE, AND BLACK TEXTS, RESPECTIVELY.

Model	Synthetic Datasets								Authentic Datasets							
	LIVE		CSIQ		TID2013		Kadid10k		LIVE-C		KonIQ10k		LIVE-FB		SPAQ	
	SROCC	PLCC	SROCC	PLCC	SROCC	PLCC	SROCC	PLCC	SROCC	PLCC	SROCC	PLCC	SROCC	PLCC	SROCC	PLCC
NIQE [36]	<b>0.903</b>	<b>0.906</b>	0.642	0.727	0.308	0.419	0.380	0.442	0.446	0.469	0.527	0.532	0.203	0.262	0.700	0.712
IL-NIQE [68]	0.878	0.884	<b>0.848</b>	<b>0.883</b>	0.504	0.636	0.557	0.599	0.427	0.481	0.511	0.532	0.234	0.286	0.713	0.724
CL-MI [5]	0.749	0.731	0.619	0.615	0.249	0.317	0.518	0.529	0.494	0.480	0.664	0.653	0.290	0.322	0.701	0.701
MD-FS [39]	<b>0.926</b>	<b>0.930</b>	0.797	0.829	0.554	0.657	0.608	0.634	0.427	0.467	0.739	0.746	0.360	0.407	0.805	0.812
CONTRIQUE-OU [34]	0.841	0.840	0.684	0.700	0.321	0.344	0.552	0.564	0.348	0.364	0.651	0.637	0.321	0.341	0.677	0.685
ReIQA-OU [44]	0.781	0.779	0.713	0.725	0.284	0.339	0.516	0.534	0.379	0.288	0.580	0.568	0.350	0.341	0.613	0.616
ARNIQA-OU [3]	0.853	0.852	0.832	0.810	0.467	0.527	0.632	0.638	0.468	0.557	0.746	0.762	<b>0.428</b>	0.468	0.788	0.797
CLIP-IQA [51]	0.626	0.651	0.748	0.805	0.525	0.632	0.465	0.473	0.656	0.670	0.695	0.730	0.344	<b>0.473</b>	0.733	0.734
GRRepQ-OU [46]	0.714	0.698	0.740	0.742	0.423	0.565	0.416	0.463	<b>0.722</b>	<b>0.766</b>	<b>0.776</b>	<b>0.798</b>	0.289	0.423	0.802	0.805
QualiCLIP [1]	0.898	0.885	0.804	0.842	<b>0.651</b>	<b>0.732</b>	<b>0.654</b>	<b>0.664</b>	<b>0.725</b>	<b>0.802</b>	<b>0.817</b>	<b>0.838</b>	<b>0.442</b>	<b>0.556</b>	<b>0.841</b>	<b>0.851</b>
HiRQA (ours)	0.902	0.890	<b>0.862</b>	<b>0.874</b>	<b>0.679</b>	<b>0.697</b>	<b>0.761</b>	<b>0.733</b>	<b>0.692</b>	<b>0.744</b>	<b>0.802</b>	<b>0.812</b>	<b>0.421</b>	<b>0.490</b>	<b>0.859</b>	<b>0.860</b>
HiRQA-S	<b>0.910</b>	<b>0.897</b>	<b>0.835</b>	<b>0.844</b>	<b>0.642</b>	<b>0.677</b>	<b>0.750</b>	<b>0.731</b>	0.632	0.701	0.768	0.782	0.397	0.466	<b>0.839</b>	<b>0.846</b>

are pooled via an attention-based pooling layer into a 1024-dimensional embedding that encodes perceptual quality characteristics. It is then passed to a fully connected *decision layer* to predict the final quality score  $q$ .

#### E. Implementation details

We implement HiRQA using PyTorch and train on 2 NVIDIA A100 GPUs for only 3 epochs. The model is optimized with the AdamW optimizer, starting with a learning rate of  $3e^{-6}$  and a weight decay of  $1e^{-5}$ . A Cosine Annealing Learning Rate Scheduler is used, which reduces the Learning rate to a minimum of  $8e^{-7}$  over 7000 iterations. *HiRQA* uses ResNet-50 as its backbone, while the lightweight *HiRQA-S* employs a ResNet-18 backbone for real-time inference.

The training data comprises a diverse set of degraded images generated from the 140 K pristine images in the KADIS700k dataset. As per the image degradation model (see Sec. III-C), multiple degradations are applied sequentially, up to a maximum  $L_{\text{dist}} = 7$  per image. Distortion intensities  $d_i$  are sampled continuously by interpolating between discrete levels defined in KADID-10k. This sampling process incorporates a Gaussian offset with zero mean and standard deviation  $\sigma_{\text{off}}^2 = 0.3$ , for subtle variations in distortion severity. For each pristine image, we randomly apply multiple distortions 5 times, generating 5 distinct distorted samples per image. This results in approximately 700K distorted images used per epoch during training.

During training, crops of size  $384 \times 384$  pixels are extracted from each image. During evaluation, we use full-resolution images and the complete dataset without any splitting. However, for SPAQ, due to its high-resolution images, we resize each image such that its shortest side is 768 pixels while preserving the original aspect ratio.

## IV. EXPERIMENTAL RESULTS AND DISCUSSION

We validate the effectiveness of the proposed HiRQA framework through a comprehensive set of experiments; our evaluation plan involves the following:

- 1) **Zero-shot benchmark evaluation.** We assess how well HiRQA correlates with human visual perception by evaluating it on standard IQA benchmarks. We conduct experiments across eight datasets: LIVE [45], CSIQ [25], TID2013 [40], Kadid10k [30], LIVE Challenge [17], KonIQ10k [21], LIVE-FB [64], and SPAQ [15]. We use the

standard metrics [56], [67]: Spearman’s rank order correlation coefficient (SROCC) and Pearson’s linear correlation coefficient (PLCC) to evaluate the correlation between the predicted and ground truth scores. PLCC is defined as

$$PLCC = \frac{\sum_{i=1}^N (\hat{q}_i - \bar{\hat{q}})(q_i - \bar{q})}{\sqrt{\sum_{i=1}^N (\hat{q}_i - \bar{\hat{q}})^2} \sqrt{\sum_{i=1}^N (q_i - \bar{q})^2}}$$

where  $N$  is the number of distorted images,  $\hat{q}_i$  is the predicted scores,  $q_i$  is the true scores;  $\bar{\hat{q}}$  and  $\bar{q}$  are the corresponding means. Besides, SROCC is defined as:

$$SROCC = 1 - \frac{6 \sum_{i=1}^N d_i^2}{N(N^2 - 1)}$$

where  $d_i$  is the pairwise differences between  $q_i$  and  $\hat{q}_i$ .

- 2) **Ablation study.** We perform experiments to analyze the contributions of individual loss terms and evaluate our proposed ranking loss for IQA learning.
- 3) **Feature visualization.** We use t-SNE to visualize the learned feature embeddings of HiRQA, offering insights into the perceptual structure captured by the model and the quality-aware clustering behavior.
- 4) **Generalization performance.** To assess the robustness of HiRQA to out-of-distribution distortions, we evaluate its performance on enhancement datasets [4], [13], [14], [38] using a density separation criterion [42].

#### A. Zero-shot benchmark evaluation

We compare HiRQA with several SOTA OU-NRIQA models, including traditional statistical approaches [36], [68]), self-supervised models [3], [5], [34], [44], and VLM frameworks [1], [46], [51]. As noted in [1], self-supervised models rely on a NIQE-style framework that measures the distance between features of distorted images and those from a corpus of pristine references to compute the quality score.

As shown in Table I, HiRQA delivers consistently strong performance across all eight IQA benchmark datasets, achieving top-three rankings in both SROCC and PLCC across all test sets. It attains the highest scores on TID2013, Kadid10k, CSIQ, and SPAQ, and offers competitive scores on authentic datasets such as LIVE-C, KonIQ10k, and LIVE-FB. Notably, this performance is achieved using a single ResNet-50 backbone without relying on auxiliary modalities or reference images during inference.



Unlike methods such as GRepQ, which utilize a dual-encoder architecture, or ARNIQA, which operates on both full and half-resolution images, HiRQA achieves superior performance with a single image encoder operating on full-resolution images, avoiding multi-resolution inputs or multi-branch networks. While models like QualiCLIP and GRepQ fine-tune CLIP encoders, that are already known to exhibit strong zero-shot capabilities for IQA [51], HiRQA is trained using a ResNet backbone pretrained on ImageNet and leverages only a text-encoder-based loss during training. Our method eliminates the dependency on large VLMs, yet consistently matches or outperforms these SOTA models across multiple benchmarks.

HiRQA also offers architectural flexibility over existing CLIP-based methods. For instance, methods such as QualiCLIP and GRepQ are inherently constrained by the CLIP architecture, offering limited flexibility in backbone selection since the vision encoder must remain compatible with CLIP’s pertaining. In contrast, HiRQA can be used with any standard backbone architecture. We demonstrate this by **HiRQA-S**, which uses a lightweight ResNet-18 as its backbone and achieves a real-time inference at just 3.5 ms per image. As presented in Table I, HiRQA-S attains competitive performance even with a much smaller backbone, demonstrating the efficiency of our design.

### B. Ablation Experiments

We conduct comprehensive ablation studies to quantify the contribution of key components within the HiRQA framework. We investigate the role of each loss function and compare our proposed higher-order ranking strategy (Pair-of-Pairs) with traditional pairwise approaches such as RankNet and Margin loss. The results are summarized in Table II-III.

**Contributions of Loss Terms.** We conduct an ablation study on the KonIQ-10k dataset by selectively enabling the ranking loss  $\mathcal{L}_{\text{ranking}}$ , the embedding distance loss  $\mathcal{L}_{\text{embdist}}$ , and the text-image alignment loss  $\mathcal{L}_{\text{align}}$ . As the results in Table II demonstrate, using only  $\mathcal{L}_{\text{ranking}}$  serves as a baseline for relative ordering among distorted images. This improves the model’s ability to rank image quality, as reflected in higher SROCC. However, it lacks explicit supervision for the magnitude of the predicted scores, leading to slightly lower PLCC scores.

To structure the learned embedding space, we incorporate the embedding loss  $\mathcal{L}_{\text{embdist}}$ , which supervises the differences in predicted quality scores based on embedding similarity. This encourages the magnitude of predicted scores to better reflect perceptual differences, leading to a 1.9% (3.01%) improvement in SROCC (PLCC) over the baseline. Similarly,

TABLE II  
ABLATION RESULTS ON KONIQ10K DATASET ARE SHOWN FOR FOUR CONFIGURATIONS OF THE PROPOSED HiRQA MODEL.

Cfg	$\mathcal{L}_{\text{ranking}}$	$\mathcal{L}_{\text{embdist}}$	$\mathcal{L}_{\text{Align}}$	SROCC	PLCC
#1	✓			0.751	0.730
#2	✓	✓		0.765	0.752
#3	✓		✓	0.782	0.771
#4	✓	✓	✓	<b>0.802</b>	<b>0.812</b>

TABLE III  
ABLATION ON RANKING FORMULATION IN HiRQA; RESULTS ARE SHOWN FOR LIVE-C AND KONIQ10K DATASETS.

Test on →	LIVE-C		KonIQ10K	
Ranking Loss	SROCC	PLCC	SROCC	PLCC
Pairwise RankNet	0.557	0.568	0.701	0.743
Margin Loss	0.640	0.703	0.757	0.775
<b>Pair-of-Pairs (ours)</b>	<b>0.692</b>	<b>0.744</b>	<b>0.802</b>	<b>0.812</b>

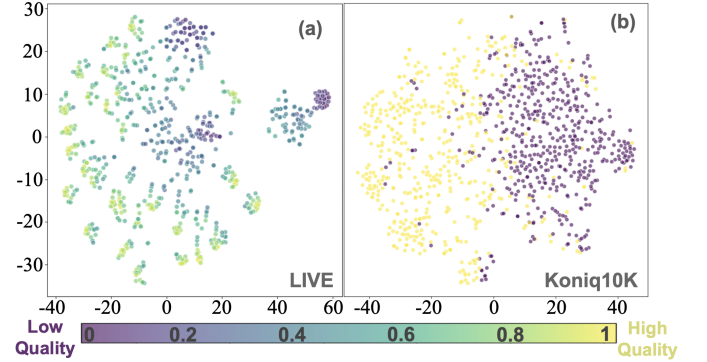


Fig. 6. t-SNE visualization of HiRQA’s learned embeddings on (a) LIVE and (b) KonIQ10K. The results highlight HiRQA’s ability to learn a perceptually structured and separable feature space.

introducing the text-image alignment loss  $\mathcal{L}_{\text{align}}$  guides the model using weak semantic supervision, improving SROCC (PLCC) by 4.1% (5.6%). This shows that aligning image features with distortion-aware text prompts provides additional structure that benefits both ranking and magnitude of the predicted scores. When all three loss terms are combined, HiRQA achieves the best performance with a 6.8%(11.1%) increase in SROCC (PLCC) compared to the baseline scores.

**Ranking Loss Variants.** We also compare three ranking loss strategies to understand their effect on learning quality-aware representations. The standard pairwise RankNet loss encourages correct ordering between image pairs but lacks global structural context, resulting in limited performance. A margin-based loss, which enforces both correct ranking and a minimum perceptual separation between predicted scores, yields stronger supervision and leads to notable gains, improving SROCC (PLCC) by 14.9% (23.7%) on LIVE-C and 7.9% (9.3%) on KonIQ10K, respectively.

Our proposed pair-of-pairs loss captures higher-order ranking relationships by comparing relative score differences across multiple pairs, thereby providing richer structural supervision. This results in improvements in SROCC (PLCC) by 24.2% (28.5%) on LIVE-C, and 14.2% (9.2%) on KonIQ-10K. These findings validate our intuition that incorporating higher-order ranking constraints leads to better perceptual alignment across datasets.

### C. Feature Visualization

We now investigate the hierarchical feature space we aimed to learn. We use t-distributed stochastic neighbor embedding (t-SNE [50]) to visualize the high-dimensional feature representations of HiRQA in a 2D space. In Fig. 6, we present t-SNE visualizations of distorted image embeddings from two datasets: LIVE and KonIQ10K. For the LIVE dataset (Fig. 6a),

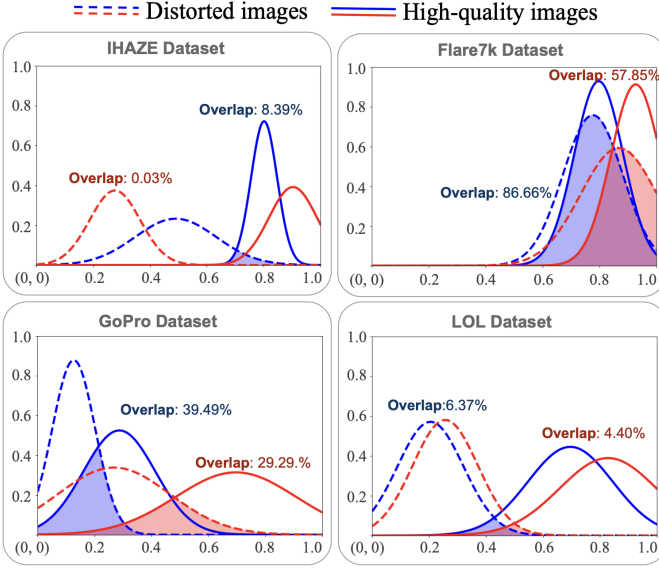


Fig. 7. Density separation by predicted IQA scores for high-quality and distorted images on Flare7K, GoPro, and IHAZE datasets. HiRQA (red) exhibits the least overlap across all cases, indicating superior generalization compared to QualiCLIP (blue).

which contains synthetically distorted images, we visualize all distorted images colored by their ground truth Mean Opinion Scores (MOS). A clear quality gradient is observed where high- and low-quality images cluster separately. This confirms that HiRQA learns a structured, quality-aware feature space, where perceptually similar images are placed closer together.

For Konqi10K (Fig. 6b), which comprises authentically distorted images, due to its large scale, we randomly sample 500 high and low-quality images based on their ground truth MOS scores and assign binary labels. From the visualization, the two groups are distinguishable in the learned space, highlighting HiRQA’s ability to generalize to complex, in-the-wild distortions. Together, these results confirm that HiRQA captures meaningful, hierarchical quality representations across both synthetic and authentic domains, aligning well with human visual perception.

#### D. Generalization to Real-World Distortions

To further demonstrate HiRQA’s generalization capability, we evaluate its performance on unseen distortions using the density separation criterion [42]. The intuition here is that a well-generalizing model should predict distinct score distributions for high- and low-quality images. Since HiRQA is trained exclusively on synthetically degraded images from KADIS-700k dataset, this metric allows us to assess how well the model transfers to real-world distortions.

We use four benchmark datasets from different domains to evaluate this: (i) IHAZE [4], which features hazy and corresponding haze-free images collected in controlled indoor settings; (ii) Flare7K [14], which contains images with synthetically added lens flare that is often subtle and difficult to distinguish; (iii) GoPro [38], which includes paired clean and motion-blurred images captured using a high-speed camera; and (iv) LOL [13] consists of low-light and corresponding well-lit images captured indoor. As a baseline, we compare

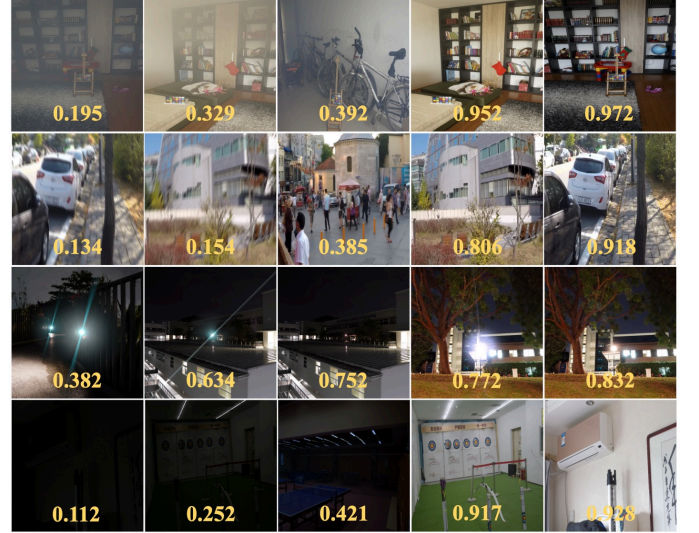


Fig. 8. Predicted quality scores by HiRQA for haze (row 1), motion blur (row 2), flare (row 3), and low-light (row 4) distortions. In each row, distortion severity increases from right to left; as shown, the corresponding quality scores of HiRQA also decrease in that order – validating its effectiveness on out-of-distribution data.

HiRQA against QualiCLIP, which is the current SOTA OU-NRIQA metric. Since IHAZE contains 4K-resolution images, we resize the shorter side to 768 pixels while preserving the aspect ratio before evaluation.

As shown in Fig. 7, HiRQA consistently achieves considerably lower overlaps between the predicted score distributions of high- and low-quality image sets compared to QualiCLIP across all datasets. Specifically, HiRQA reduces the overlap by 28.81% on Flare7K, 10.20% on GoPro, 1.97% on LOL, and achieves almost disjoint separation with only 0.03% overlap on IHAZE. This strong separation across a range of distortion types, including global distortions like haziness and low-light as well as localized effects like flare and motion-blur, demonstrates the robustness of HiRQA and how it is able to generalize to real-world distortions beyond training datasets.

Furthermore, Fig. 8 shows some representative examples from the datasets used in the density separation analysis, with HiRQA’s predicted scores decreasing consistently as distortion severity increases in unseen images across haze, motion blur, flare, and low-light conditions.

**Limitations and Future Work.** While HiRQA demonstrates strong generalization and SOTA performance in OU NRIQA, the training relies on a simplifying assumption. For images with multiple distortions, we assume that the overall distortion severity corresponds to the maximum distortion level among the applied transformations. This may not always reflect perceptual dominance, especially when multiple moderate distortions jointly degrade quality. As a result, the current formulation does not fully capture the cumulative effect of multiple distortions.

Moreover, like other OU-NRIQA models, HiRQA still lags behind some fully supervised counterparts. A promising future direction would be to design a distortion-aware aggregation scheme, one that jointly accounts for the maximum severity, the number, and type of distortions present. Such a refinement



could enable more accurate and perceptually consistent quality predictions, particularly in images affected by complex or compound distortions.

## V. CONCLUSION

We presented HiRQA, a novel opinion-unaware NR-IQA framework that learns a hierarchical, quality-aware embedding space using synthetic distortions and relative ranking signals. Unlike prior methods that rely on pristine reference images or pre-trained vision-language encoders, HiRQA operates using only a single distorted image and image encoder at inference. Our approach combines a higher-order pair-of-pairs ranking loss with embedding distance alignment and semantic guidance via structured text prompts during training. This self-supervised approach enables HiRQA to learn perceptually meaningful features without relying on any subjective labels. Through extensive experiments on both synthetic and authentic IQA datasets, HiRQA consistently achieves SOTA performance across multiple benchmarks. It also demonstrates superior generalization compared to real-world distortions through the density separation analysis and learns a perceptually structured embedding space, as shown through t-SNE visualizations. We further demonstrate the scalability of our framework by substituting the backbone with a light-weight variant (HiRQA-S), which achieves competitive performance while enabling real-time inference.

## ACKNOWLEDGMENT

This work is supported in part by the National Science Foundation (NSF) award #2330416 and the University of Florida research grant #132763.

## REFERENCES

- [1] Lorenzo Agnolucci, Leonardo Galteri, and Marco Bertini. Quality-aware image-text alignment for opinion-unaware image quality assessment. *arXiv preprint arXiv:2403.11176*, 2024. 1, 2, 3, 4, 6
- [2] Lorenzo Agnolucci, Leonardo Galteri, Marco Bertini, and Alberto Del Bimbo. Perceptual quality improvement in videoconferencing using keyframes-based gan. *IEEE Transactions on Multimedia*, 26:339–352, 2024. 1
- [3] Lorenzo Agnolucci, Leonardo Galteri, Marco Bertini, and Alberto Del Bimbo. Arniqa: Learning Distortion Manifold for Image Quality Assessment. In *Proceedings of the IEEE/CVF Winter Conference on Applications of Computer Vision*, pages 189–198, 2024. 2, 5, 6
- [4] Codruta O. Ancuti, Cosmin Ancuti, Radu Timofte, and Christophe De Vleeschouwer. I-HAZE: A Dehazing Benchmark With Real Hazy and Haze-Free Indoor Images. In *arXiv:1804.05091v1*, 2018. 2, 6, 8
- [5] Nithin C Babu, Vignesh Kannan, and Rajiv Soundararajan. No reference opinion unaware quality assessment of authentically distorted images. In *2023 IEEE/CVF Winter Conference on Applications of Computer Vision (WACV)*, pages 2458–2467, 2023. 1, 3, 6
- [6] Simone Bianco, Luigi Celona, Paolo Napoletano, and Raimondo Schettini. On the Use of Deep Learning for Blind Image Quality Assessment. *Signal, Image and Video Processing*, 12:355–362, 2018. 2
- [7] Sebastian Bosse, Dominique Maniry, Klaus-Robert Müller, Thomas Wiegand, and Wojciech Samek. Deep Neural Networks for No-Reference and Full-Reference Image Quality Assessment. *IEEE Transactions on image processing*, 27(1):206–219, 2017. 2
- [8] Christopher Burges, Tal Shaked, Erin Renshaw, Ari Lazier, Matt Deeds, Nicole Hamilton, and Gregory Hullender. Learning to rank using gradient descent. In *ICML 2005 - Proceedings of the 22nd International Conference on Machine Learning*, pages 89–96, 01 2005. 4
- [9] Ting Chen, Simon Kornblith, Mohammad Norouzi, and Geoffrey Hinton. A simple framework for contrastive learning of visual representations, 2020. 2
- [10] Xinlei Chen, Haoqi Fan, Ross Girshick, and Kaiming He. Improved baselines with momentum contrastive learning, 2020. 2
- [11] Zhihao Chen, Bin Hu, Chuang Niu, Tao Chen, Yuxin Li, Hongming Shan, and Ge Wang. Iqaqpt: Image quality assessment with vision-language and chatgpt models, 2023. 3
- [12] Zheng Chen, Xun Zhang, Wenbo Li, Renjing Pei, Fenglong Song, Xiongkuo Min, Xiaohong Liu, Xin Yuan, Yong Guo, and Yulun Zhang. Grounding-iqa: Multimodal language grounding model for image quality assessment, 2025. 3
- [13] Chen Wei, Wenjing Wang, Wenhan Yang, Jiaying Liu. Deep Retinex Decomposition for Low-Light Enhancement. In *British Machine Vision Conference*, 2018. 2, 6, 8
- [14] Yuekun Dai, Chongyi Li, Shangchen Zhou, Ruicheng Feng, and Chen Change Loy. Flare7K: A Phenomenological Nighttime Flare Removal Dataset. In *Thirty-sixth Conference on Neural Information Processing Systems Datasets and Benchmarks Track*, 2022. 2, 6, 8
- [15] Yuming Fang, Hanwei Zhu, Yan Zeng, Kede Ma, and Zhou Wang. Perceptual quality assessment of smartphone photography. In *IEEE Conference on Computer Vision and Pattern Recognition*, pages 3677–3686, 2020. 1, 2, 6
- [16] Xinbo Gao, Fei Gao, Dacheng Tao, and Xuelong Li. Universal Blind Image Quality Assessment Metrics Via Natural Scene Statistics and Multiple Kernel Learning. *IEEE Transactions on neural networks and learning systems*, 24(12), 2013. 2
- [17] Deepti Ghadiyaram and Alan C Bovik. Massive Online Crowdsourced Study of Subjective and Objective Picture Quality. *IEEE Transactions on Image Processing*, 25(1):372–387, 2015. 2, 6
- [18] Deepti Ghadiyaram and Alan C Bovik. Perceptual Quality Prediction on Authentically Distorted Images Using a Bag of Features Approach. *Journal of vision*, 17(1):32–32, 2017. 2
- [19] S Alireza Golestaneh, Saba Dadsetan, and Kris M Kitani. No-Reference Image Quality Assessment Via Transformers, Relative Ranking, and Self-Consistency. In *Proceedings of the IEEE/CVF winter conference on applications of computer vision*, pages 1220–1230, 2022. 2
- [20] Kaiming He, Xiangyu Zhang, Shaoqing Ren, and Jian Sun. Deep residual learning for image recognition, 2015. 3
- [21] Vlad Hosu, Hanhe Lin, Tamas Sziranyi, and Dietmar Saupe. KonIQ-10k: An Ecologically Valid Database for Deep Learning of Blind Image Quality Assessment. *IEEE Transactions on Image Processing*, 29:4041–4056, 2020. 2, 6
- [22] Tao Jiang, Xiao-juan Hu, Xing-hua Yao, Li-ping Tu, Jing-bin Huang, Xu-xiang Ma, Ji Cui, Qing-feng Wu, and Jia-tuo Xu. Tongue Image Quality Assessment Based on a Deep Convolutional Neural Network. *BMC Medical Informatics and Decision Making*, 21(1):147, 2021. 2
- [23] Le Kang, Peng Ye, Yi Li, and David Doermann. Convolutional Neural Networks for No-Reference Image Quality Assessment. In *Proceedings of the IEEE conference on computer vision and pattern recognition*, pages 1733–1740, 2014. 2
- [24] Junjie Ke, Qifei Wang, Yilin Wang, Peyman Milanfar, and Feng Yang. Musiq: Multi-Scale Image Quality Transformer. In *Proceedings of the IEEE/CVF international conference on computer vision*, pages 5148–5157, 2021. 2
- [25] Eric C Larson and Damon M Chandler. Most Apparent Distortion: Full-Reference Image Quality Assessment and The Role of Strategy. *Journal of electronic imaging*, 19(1):011006–011006, 2010. 2, 6
- [26] Dongxu Li, Junnan Li, Hung Le, Guangsen Wang, Silvio Savarese, and Steven C.H. Hoi. LAVIS: A one-stop library for language-vision intelligence. In *Proceedings of the 61st Annual Meeting of the Association for Computational Linguistics (Volume 3: System Demonstrations)*, pages 31–41, Toronto, Canada, July 2023. Association for Computational Linguistics. 5
- [27] Junnan Li, Dongxu Li, Caiming Xiong, and Steven Hoi. Blip: Bootstrapping language-image pre-training for unified vision-language understanding and generation. In *ICML*, 2022. 5
- [28] Xudong Li, Zihao Huang, Runze Hu, Yan Zhang, Liujuan Cao, and Rongrong Ji. Boosting clip adaptation for image quality assessment via meta-prompt learning and gradient regularization, 2024. 2
- [29] Jingyun Liang, Jiezhang Cao, Guolei Sun, Kai Zhang, Luc Van Gool, and Radu Timofte. Swinir: Image Restoration Using Swin Transformer. In *Proceedings of the IEEE/CVF international conference on computer vision*, pages 1833–1844, 2021. 1
- [30] Hanhe Lin, Vlad Hosu, and Dietmar Saupe. KADID-10k: A Large-Scale Artificially Distorted IQA Database. In *Eleventh International Conference on Quality of Multimedia Experience (QoMEX)*, pages 1–3. IEEE, 2019. 2, 5, 6
- [31] Hanhe Lin, Vlad Hosu, and Dietmar Saupe. Deepfl-iqa: Weak supervision for deep iqa feature learning. *arXiv preprint arXiv:2001.08113*, 2020. 5
- [32] Kwan-Yee Lin and Guanxiang Wang. Hallucinated-IQA: No-Reference Image Quality Assessment Via Adversarial Learning. In *Proceedings of the IEEE conference on computer vision and pattern recognition*, pages

- 732–741, 2018. **2**
- [33] Kede Ma, Wentao Liu, Tongliang Liu, Zhou Wang, and Dacheng Tao. dipIQ: Blind Image Quality Assessment by Learning-to-Rank Discriminable Image Pairs. *IEEE Transactions on Image Processing*, 26(8):3951–3964, 2017. **3**
- [34] Pavan C Madhusudana, Neil Birkbeck, Yilin Wang, Balu Adsumilli, and Alan C Bovik. Image quality assessment using contrastive learning. *arXiv:2110.13266*, 2021. **2, 5, 6**
- [35] Anish Mittal, Anush Krishna Moorthy, and Alan Conrad Bovik. No-Reference Image Quality Assessment in the Spatial Domain. *IEEE Transactions on image processing*, 21(12):4695–4708, 2012. **2**
- [36] Anish Mittal, Rajiv Soundararajan, and Alan C. Bovik. Making a “completely blind” image quality analyzer. *IEEE Signal Processing Letters*, 20(3):209–212, 2013. **1, 3, 6**
- [37] Anush Krishna Moorthy and Alan Conrad Bovik. Blind Image Quality Assessment: From Natural Scene Statistics to Perceptual Quality. *IEEE transactions on Image Processing*, 20(12):3350–3364, 2011. **2**
- [38] Seungjun Nah, Tae Hyun Kim, and Kyoung Mu Lee. Deep Multi-Scale Convolutional Neural Network for Dynamic Scene Deblurring. In *Proceedings of the IEEE conference on computer vision and pattern recognition*, pages 3883–3891, 2017. **2, 6, 8**
- [39] Zhangkai Ni, Yue Liu, Keyan Ding, Wenhan Yang, Hanli Wang, and Shiqi Wang. Opinion-unaware blind image quality assessment using multi-scale deep feature statistics, 2024. **3, 6**
- [40] Nikolay Ponomarenko, Lina Jin, Oleg Ieremeiev, Vladimir Lukin, Karen Egiazarian, Jaakko Astola, Benoit Vozel, Kacem Chehdi, Marco Carli, Federica Battisti, et al. Image Database TID2013: Peculiarities, Results and Perspectives. *Signal processing: Image communication*, 30:57–77, 2015. **2, 6**
- [41] Alec Radford, Jong Wook Kim, Chris Hallacy, Aditya Ramesh, Gabriel Goh, Sandhini Agarwal, Girish Sastry, Amanda Askell, Pamela Mishkin, Jack Clark, Gretchen Krueger, and Ilya Sutskever. Learning transferable visual models from natural language supervision, 2021. **2, 3, 4**
- [42] Vaishnav Ramesh, Junliang Liu, Haining Wang, and Md Jahidul Islam. Dgqa: Depth-guided feature attention and refinement for generalizable image quality assessment, 2025. **2, 6, 8**
- [43] Michele A Saad, Alan C Bovik, and Christophe Charrier. Blind Image Quality Assessment: A Natural Scene Statistics Approach in the DCT Domain. *IEEE transactions on Image Processing*, 21(8):3339–3352, 2012. **2**
- [44] Avinab Saha, Sandeep Mishra, and Alan C Bovik. Re-iqa: Unsupervised Learning for Image Quality Assessment In the Wild. In *Proceedings of the IEEE/CVF conference on computer vision and pattern recognition*, pages 5846–5855, 2023. **2, 5, 6**
- [45] Hamid R Sheikh, Muhammad F Sabir, and Alan C Bovik. A Statistical Evaluation of Recent Full Reference Image Quality Assessment Algorithms. *IEEE Transactions on image processing*, 15(11):3440–3451, 2006. **2, 6**
- [46] Suhas Srinath, Shankhanil Mitra, Shika Rao, and Rajiv Soundararajan. Learning generalizable perceptual representations for data-efficient no-reference image quality assessment. In *Proceedings of the IEEE/CVF Winter Conference on Applications of Computer Vision (WACV)*, pages 22–31, January 2024. **1, 2, 3, 6**
- [47] Shaolin Su, Qingsen Yan, Yu Zhu, Cheng Zhang, Xin Ge, Jinqiu Sun, and Yanning Zhang. Blindly Assess Image Quality in the Wild Guided by a Self-Adaptive Hyper Network. In *Proceedings of the IEEE/CVF conference on computer vision and pattern recognition*, pages 3667–3676, 2020. **2**
- [48] Hossein Talebi and Peyman Milanfar. NIMA: Neural Image Assessment. *IEEE transactions on image processing*, 27(8):3998–4011, 2018. **2**
- [49] Aaron van den Oord, Yazhe Li, and Oriol Vinyals. Representation learning with contrastive predictive coding, 2019. **5**
- [50] Laurens Van der Maaten and Geoffrey Hinton. Visualizing Data Using t-SNE. *Journal of machine learning research*, 9(11), 2008. **7**
- [51] Jianyi Wang, Kelvin CK Chan, and Chen Change Loy. Exploring Clip for Assessing the Look and Feel of Images. In *Proceedings of the AAAI Conference on Artificial Intelligence*, volume 37, pages 2555–2563, 2023. **1, 2, 3, 4, 6, 7**
- [52] Lanjiang Wang. A Survey on IQA. *arXiv preprint arXiv:2109.00347*, 2021. **1**
- [53] Xintao Wang, Liangbin Xie, Chao Dong, and Ying Shan. Real-esrgan: Training Real-world Blind Super-resolution With Pure Synthetic Data. In *Proceedings of the IEEE/CVF international conference on computer vision*, pages 1905–1914, 2021. **1**
- [54] Zhou Wang and Alan Conrad Bovik. *Modern Image Quality Assessment*. PhD thesis, Springer, 2006. **1**
- [55] Zhou Wang, Alan C Bovik, and Ligang Lu. Why Is Image Quality Assessment So Difficult? In *IEEE International conference on acoustics, speech, and signal processing*, volume 4, pages IV–3313. IEEE, 2002. **1**
- [56] Zhou Wang, Alan C Bovik, Hamid R Sheikh, and Eero P Simoncelli. Image Quality Assessment: From Error Visibility to Structural Similarity. *IEEE transactions on image processing*, 13(4):600–612, 2004. **6**
- [57] Haoning Wu, Zicheng Zhang, Erli Zhang, Chaofeng Chen, Liang Liao, Annan Wang, Chunyi Li, Wenxiu Sun, Qiong Yan, Guangtao Zhai, and Weisi Lin. Q-bench: A benchmark for general-purpose foundation models on low-level vision, 2024. **3**
- [58] Haoning Wu, Zicheng Zhang, Weixia Zhang, Chaofeng Chen, Chunyi Li, Liang Liao, Annan Wang, Erli Zhang, Wenxiu Sun, Qiong Yan, Xiongkuo Min, Guangtai Zhai, and Weisi Lin. Q-align: Teaching Imms for visual scoring via discrete text-defined levels. *arXiv preprint arXiv:2312.17090*, 2023. Equal Contribution by Wu, Haoning and Zhang, Zicheng. Project Lead by Wu, Haoning. Corresponding Authors: Zhai, Guangtai and Lin, Weisi. **3**
- [59] Tianhe Wu, Kede Ma, Jie Liang, Yujiu Yang, and Lei Zhang. A Comprehensive Study of Multimodal Large Language Models for Image Quality Assessment. *arXiv preprint arXiv:2403.10854*, 2024. **3**
- [60] Jingtao Xu, Peng Ye, Qiaohong Li, Haiqing Du, Yong Liu, and David Doermann. Blind Image Quality Assessment Based on High Order Statistics Aggregation. *IEEE Transactions on Image Processing*, 25(9):4444–4457, 2016. **2**
- [61] Sidi Yang, Tianhe Wu, Shuwei Shi, Shanshan Lao, Yuan Gong, Mingdeng Cao, Jiahao Wang, and Yujiu Yang. Maniqa: Multi-Dimension Attention Network for No-Reference Image Quality Assessment. In *Proceedings of the IEEE/CVF Conference on Computer Vision and Pattern Recognition*, pages 1191–1200, 2022. **2**
- [62] Peng Ye and David Doermann. No-Reference Image Quality Assessment Using Visual Codebooks. *IEEE Transactions on Image Processing*, 21(7):3129–3138, 2012. **2**
- [63] Peng Ye, Jayant Kumar, Le Kang, and David Doermann. Unsupervised Feature Learning Framework for No-Reference Image Quality Assessment. In *IEEE conference on computer vision and pattern recognition*, pages 1098–1105. IEEE, 2012. **2**
- [64] Zhenqiang Ying, Haoran Niu, Praful Gupta, Dhruv Mahajan, Deepti Ghadiyaram, and Alan Bovik. From Patches to Pictures (PaQ-2-PiQ): Mapping the Perceptual Space of Picture Quality. In *Proceedings of the IEEE/CVF conference on computer vision and pattern recognition*, pages 3575–3585, 2020. **2, 6**
- [65] Junyong You and Jari Korhonen. Transformer for Image Quality Assessment. In *IEEE international conference on image processing (ICIP)*, pages 1389–1393. IEEE, 2021. **2**
- [66] Zhiyuan You, Zheyuan Li, Jinjin Gu, Zhenfei Yin, Tianfan Xue, and Chao Dong. Depicting beyond scores: Advancing image quality assessment through multi-modal language models, 2024. **3**
- [67] Guangtao Zhai and Xiongkuo Min. Perceptual Image Quality Assessment: A Survey. *Science China Information Sciences*, 63:1–52, 2020. **6**
- [68] Lin Zhang, Lei Zhang, and Alan C. Bovik. A feature-enriched completely blind image quality evaluator. *IEEE Transactions on Image Processing*, 24(8):2579–2591, 2015. **1, 3, 6**
- [69] Weixia Zhang, Kede Ma, Jia Yan, Dexiang Deng, and Zhou Wang. Blind Image Quality Assessment Using a Deep Bilinear Convolutional Neural Network. *IEEE Transactions on Circuits and Systems for Video Technology*, 30(1):36–47, 2018. **2**
- [70] Weixia Zhang, Guangtao Zhai, Ying Wei, Xiaokang Yang, and Kede Ma. Blind image quality assessment via vision-language correspondence: A multitask learning perspective. In *IEEE Conference on Computer Vision and Pattern Recognition*, pages 14071–14081, 2023. **2, 3, 4**
- [71] Kai Zhao, Kun Yuan, Ming Sun, Mading Li, and Xing Wen. Quality-aware pretrained models for blind image quality assessment. In *CVPR*, pages 22302–22313. IEEE, 2023. **2, 5**
- [72] Fei Zhou, Tianhao Gu, Zhicong Huang, and Guoping Qiu. Vision language modeling of content, distortion and appearance for image quality assessment, 2024. **2, 3, 4**
- [73] Hancheng Zhu, Leida Li, Jinjian Wu, Weisheng Dong, and Guangming Shi. MetaQA: Deep Meta-Learning for No-Reference Image Quality Assessment. In *Proceedings of the IEEE/CVF conference on computer vision and pattern recognition*, pages 14143–14152, 2020. **2**